RESEARCH ARTICLE

Multiscalar Control Based Airgap Flux Optimization of Induction Motor for Loss Minimization

TADELE AYANA, **MARCIN MORAWIEC, (Senior Member, IEEE), AND LELISA WOGI**
Faculty of Electrical and Control Engineering, Gdańsk University of Technology, 80-233 Gdańsk, Poland

Corresponding author: Tadele Ayana (tadele.ayana@pg.edu.pl)

ABSTRACT Based on the induction motor model, considering the core loss resistance that accounts for magnetic characteristic saturation, a speed control approach is devised with an adaptive full-order (AFO) speed observer. The induction motor model analysis is done sincerely in a stationary reference frame. The control approach incorporates a flux reference generator designed to meet optimal operational circumstances and a nonlinear speed controller. The machine state variables are involved in flux generation and speed control rules. The performance of the proposed control strategy is formally studied by simulation and demonstrated through experiments. The technique exhibits fast convergence to the optimal flux level, reduces computational resource requirements, and enhances torque production and loss minimization accuracy. It eliminates the excessive flux demands compared to open-loop steady-state values, which will necessitate greater current levels without justification, resulting in an increased power dissipated. This optimum flux level minimizes induction motor losses for efficiency increments.

I. INTRODUCTION

Sensorless speed control can save costs, prevent mechanical speed sensor fragility, and eliminate the inconvenience of placing the sensor in various applications. As a result, its application in industry is gaining traction. Due to the high order, multiple variables, and nonlinearity of induction motor (IM) dynamics, estimating rotor speed and flux without measuring mechanical variables remains difficult.

Accurate velocity data holds significant importance in managing the speed of induction motor (IM) drives. For measuring speed, one uses encoders or direct speed sensors. However, they have several drawbacks, including more expense, space, wiring, cautious mounting, and electronics. Sensorless IM drive speed estimation techniques were created to replace the direct speed sensors [1]. Low cost, outstanding dependability, smaller size, less maintenance, fewer wires, and less complexity are the attributes of sensorless drives.

The flux level affects resistive and core losses in variable-speed induction motor (IM) drives. Numerous methods for minimizing losses have been devised to modify the flux level based on the motor load and velocity. The techniques can be separated into two groups: Online search power controllers measure the input power and continuously change the flux level until they find the minimum amount of input power. Although they are not affected by the parameters of the motor, they frequently converge slowly, which could result in pulsations of torque and flux. Loss-model-based controllers (LMC) use functional loss models to assess the optimal level of flow.

Finding explicit controllers and estimators for severely nonlinear systems is extremely difficult. Over the years, a few speed sensorless control algorithms for IM research that take iron or core loss resistance into account have been proposed in the literature.

Sensorless scalar, field-oriented, high-order sliding-mode, hybrid adaptive sliding mode [2] and [3] induction motor control with core loss have been shown. In recent years, much effort has been expended to improve the performance

---

The associate editor coordinating the review of this manuscript and approving it for publication was Giambattista Gruosso.

of induction motor drives, particularly in eliminating low and very high rotor speed sensors and boosting efficiency and dynamics. Several papers have proposed solutions to the problem of estimating state and performance parameters. An estimator is used to recreate the values of the state variables and the rotor angular speed or position. Additional harmonics from PWM inverter parameters are also present in electrical machines, and these additional harmonics will result in further machine losses. The PWM technique involves varying the width of an intermediate circuit, similar to the regulated voltage of DC/DC voltage pulses. This allows for the synthesis of waveforms for both voltage and current, as well as the control of their fundamental harmonic frequencies and rms values [4]. In [5] and [6], multiscalar nonlinear control was studied, but without core loss consideration.

The IM mathematical model underpins the commonly used speed observer structure algorithms. Algorithmic techniques include the Kalman filter [7], [8], full-order adaptive observer [9], [10], [11], [12], [13], [14], [15], [16], sliding technique structures, and backstepping structures [17]. They also present a combination of complete and reduced-order state observers. Reference [18] proposes a nonadaptive rotor speed estimation of an induction machine in an adaptive full-order observer.

The model reference adaptive system is a typical type of feedback utilized by closed-loop observers [19], [20]. These MRAS approaches are influenced by changes in stator resistance temperature and the requirement for pure integrators in their reference models.

These difficulties have limited speed sensorless vector control applications in high-performance and low-speed drives. The EKF technique has been proposed to improve estimating performance [21]. Because of its superior performance, EKF is the most appealing of these closed-loop estimators. It has been widely employed in nonlinear system state estimation and is now a standard technique.

However, this stochastic observer has some inherent drawbacks, such as noise sensitivity, computational cost, and a lack of design and tuning requirements, where systematic avoidance of these issues, such as disturbance rejection techniques or deterministic approaches, should be used.

Two types of motor efficiency-enhancing control strategies exist: search controllers (SC) and LMC. The search controller's essential operation is to measure the input power for a particular torque and speed, then repeatedly search for the flux level (or variables comparable to it) until the least amount of input power is discovered [22]. The search controller has serious shortcomings, including torque ripples and delayed convergence.

Before selecting a flux level to lower losses, the model-based controller computes losses using the machine model [23]. LMC travels swiftly and without ripples in torque. However, the accuracy of the motor drive and loss modeling is necessary to achieve the desired precision.

This paper models the induction motor with core loss resistance taken into consideration, using feedback linearization control mechanisms, and verifies its stability and performance under various load scenarios.

Fig.1. below are the basic procedures to be followed to reach the goal to design loss minimizing flux level control of IM considering core loss resistance.
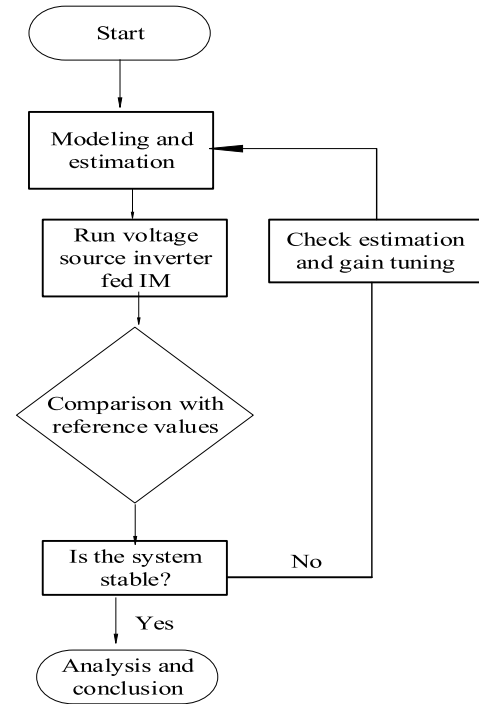

FIGURE 1. Flow chart of tested sensorless speed control of induction motor.

II. INDUCTION MOTOR MODEL

In the stationary reference frame, the vector model of the induction motor can be represented as differential equations for the stator current vector and the rotor flux vector of the following form [2]:

$$\frac{di_{s\alpha}}{dt} = a_1 i_{s\alpha} + a_2 \phi_{r\alpha} + a_3 i_{m\alpha} + a_4 u_{s\alpha}$$

$$\frac{di_{s\beta}}{dt} = a_1 i_{s\beta} + a_2 \phi_{r\beta} + a_3 i_{m\beta} + a_4 u_{s\beta} \quad (1)$$

$$\frac{d\phi_{r\alpha}}{dt} = a_5 \phi_{r\alpha} - \omega_r \phi_{r\beta} + a_6 i_{m\alpha}$$

$$\frac{d\phi_{r\beta}}{dt} = a_5 \phi_{r\beta} + \omega_r \phi_{r\alpha} + a_6 i_{m\beta} \quad (2)$$

$$\frac{di_{m\alpha}}{dt} = a_7 i_{m\alpha} + a_8 \phi_{r\alpha} + a_9 i_{s\alpha}$$

$$\frac{di_{m\beta}}{dt} = a_7 i_{m\beta} + a_8 \phi_{r\beta} + a_9 i_{s\beta} \quad (3)$$

and the motion equation

$$\frac{d\omega_r}{dt} = a_0(\phi_{r\alpha} i_{s\beta} - \phi_{r\beta} i_{s\alpha}) - \frac{T_L}{J} \quad (4)$$

where the following coefficient designations have been introduced:

$$a_0 = \frac{3L_mN_p}{2J(L_r - L_m)}, \quad a_1 = -(\frac{R_s + R_c}{L_s - L_m}),$$

$$a_2 = -\frac{R_c}{(L_s - L_m)(L_r - L_m)},$$

$$a_3 = \frac{R_cL_r}{(L_s - L_m)(L_r - L_m)}, \quad a_4 = \frac{1}{L_s - L_m},$$

$$a_5 = -\frac{R_r}{L_r - L_m}, \quad a_6 = -a_5L_m$$

$$a_7 = -\frac{R_c}{L_m}, \quad a_8 = -a_7\frac{1}{(L_r - L_m)}, \quad a_9 = -a_7$$

where T_L is load torque, N_p is the number of pole pairs, J is the rotor moment of inertia, $u_{s\alpha}$, $u_{s\beta}$ are the stator voltages, $i_{s\alpha}$, $i_{s\beta}$ are the stator currents, $i_{m\alpha}$, $i_{m\beta}$ are the magnetizing currents, $\phi_{r\alpha}$, $\phi_{r\beta}$ are the rotor fluxes, and ω_r is the rotor velocity, and moreover, R_s is stator, R_r is rotor, R_c is core resistances and L_s is stator, L_r is rotor, L_m is mutual inductance.

It should be noted that all variables and parameters used in the paper are expressed in the p.u. system. The preceding model shows that an induction motor is a nonlinear, multivariable system, and applying the above concept to the control process is complicated.

III. PROPOSED CONTROL SYSTEM

An induction-machine model with scalars and coordinate system independent state variables called the multiscalar model was first presented in [6].

In this study, firstly remodeling the induction motor model as a function of stator,magnetizing currents and airgap fluxes (i_s, i_m, ϕ_m) is mandatory to formulate the proposed control strategy.

$$\frac{d\phi_{m\alpha}}{dt} = \frac{L_m}{L_r}\frac{d\phi_{r\alpha}}{dt} + \frac{L_m(L_r - L_m)}{L_r}\frac{di_{s\alpha}}{dt}$$

$$\frac{d\phi_{m\beta}}{dt} = \frac{L_m}{L_r}\frac{d\phi_{r\beta}}{dt} + \frac{L_m(L_r - L_m)}{L_r}\frac{di_{s\beta}}{dt} \quad (5)$$

It is possible to derive equation (5) by using equations (1) and (2). Now, the former equations will have the following general form of equations.

$$w = [i_{s\alpha} \; i_{s\beta} \; \phi_{m\alpha} \; \phi_{m\beta} \; i_{m\alpha} \; i_{m\beta} \; \omega_r]^T \quad (6)$$

and the derivative of (6) is;

$$\dot{w} = [\dot{i}_{s\alpha} \; \dot{i}_{s\beta} \; \dot{\phi}_{m\alpha} \; \dot{\phi}_{m\beta} \; \dot{i}_{ma} \; \dot{i}_{m\beta} \; \dot{\omega}_r]^T \quad (7)$$

where $\phi_{m\alpha}$, $\phi_{m\beta}$ are the airgap fluxes.

The multiscalar variable transformation can be written as,

$$w_{11} = \omega_r$$

$$w_{12} = \phi_{m\alpha}i_{s\beta} - \phi_{m\beta}i_{s\alpha}$$

$$w_{21} = \phi^2_{m\alpha} + \phi^2_{m\beta}$$

$$w_{22} = \phi_{m\alpha}i_{s\alpha} + \phi_{m\beta}i_{s\beta} \quad (8)$$

where the rotor speed is the variable w_{11}, the electromagnetic torque is w_{12}, the square of the rotor flux is w_{21}, and the energy is somehow proportional to w_{22}.

The differential equation representing the transformed variables in (8) is written as follows

$$\frac{dw_{11}}{dt} = \frac{d\omega_r}{dt} \quad (9)$$

$$\frac{dw_{12}}{dt} = \frac{d\phi_{m\alpha}}{dt}i_{s\beta} + \frac{di_{s\beta}}{dt}\phi_{m\alpha}$$

$$- \frac{d\phi_{m\beta}}{dt}i_{s\alpha} - \frac{di_{s\alpha}}{dt}\phi_{m\beta} \quad (10)$$

$$\frac{dw_{21}}{dt} = 2\frac{d\phi_{m\alpha}}{dt}\phi_{m\alpha} + 2\frac{d\phi_{m\beta}}{dt}\phi_{m\beta} \quad (11)$$

$$\frac{dw_{22}}{dt} = \frac{d\phi_{m\alpha}}{dt}i_{s\alpha} + \phi_{m\alpha}\frac{di_{s\alpha}}{dt} + \frac{d\phi_{m\beta}}{dt}i_{s\beta} + \phi_{m\beta}\frac{di_{s\beta}}{dt} \quad (12)$$

Substituting for the right-hand side of the equations (9)-(12)

$$\frac{dw_{11}}{dt} = \frac{L_m}{JL_r}w_{12} - \frac{m_o}{J} \quad (13)$$

$$\frac{dw_{12}}{dt} = T_mw_{12} + m_1 \quad (14)$$

$$\frac{dw_{21}}{dt} = T_mw_{21} + m_2 \quad (15)$$

$$\frac{dw_{22}}{dt} = w_{11}w_{12}w_{22} + a_2w_{21}$$

$$+ a_2(\frac{w_{12}w_{12} + w_{22}w_{22}}{w_{21}})$$

$$+ a_3(\phi_{m\alpha}i_{m\alpha} + \phi_{m\beta}i_{m\beta}) \quad (16)$$

where T_m is the motor electromagnetic time constant, m_o is load moment, J is inertia, u_1 and u_2 are control variables included in m_1 and m_2 respectively. moreover, they can be expressed as;

$$T_m = \frac{R_r}{(L_r - L_m)}$$

$$u_1 = \phi_{m\alpha}u_{s\beta} - \phi_{m\beta}u_{s\alpha}$$

$$u_2 = \phi_{m\alpha}u_{s\alpha} + \phi_{m\beta}u_{s\beta} \quad (17)$$

The next task is to linearize the nonlinear system by introducing new signals against the nonlinearity in the system, which are to be computed from PI controllers.
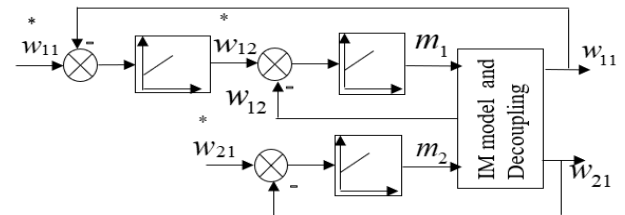

FIGURE 2. PI cascaded multiscalar model control.

The control signals m_1 and m_2 for the control system are produced by the PI controller of the state variables w_{12} and w_{21}, respectively.

The nonlinearity is compensated by (14) and (15) with thecreation of these two signals, the signals u_1 and u_2 can be calculated.

The PWM algorithm's required voltage components ($u_{s\alpha}$ and $u_{s\beta}$) are specified as;

$$u_{s\alpha} = \frac{\phi_{m\alpha}u_2 - \phi_{m\beta}u_1}{w_{21}}$$

$$u_{s\beta} = \frac{\phi_{m\alpha}u_1 + \phi_{m\beta}u_2}{w_{21}} \tag{18}$$

A. AIRGAP FLUX OPTIMIZATION

In high-performance drives, the adjustable-speed controller's primary function is to track the reference speed as quickly as possible. On the one hand, it is widely known, and will be explained in the following chapter, that induction motors should be run with a lower flux during light loads to reduce energy consumption. On the other hand, the issue that arises during light load operation is how to get the quickest response possible during a large load shift.

Therefore, the reference value of growth to the nominal level could be applied for system boundaries when the step speed command increase appears at low load and flux levels.

The associated resistance and current relationships yield the copper and core losses. Consequently, the following is how the power loss in the copper and core is expressed [24]:

$$P_L = \frac{3}{2}[R_s(i_{s\alpha}^2 + i_{s\beta}^2) + R_r(i_{r\alpha}^2 + i_{r\beta}^2) + R_c(i_{Rc\alpha}^2 + i_{Rc\beta}^2)] \tag{19}$$

where P_L stands for the total power loss of the induction motor and $i_{Rc\alpha}, i_{Rc\beta}$ are currents following through core resistance.

P_L can be thought of as a cost function because it is a positive definite function that can then be reduced using any desired variables. In this paper, since the aim of the study is to design the optimum value of flux by using a multiscalar variable that gives the lowest possible loss of induction motor that maximizes power efficiency, the air gap fluxes were taken as the desired variables to reduce the power loss cost function defined.

It is well known that motor efficiency can be increased by changing the motor flux when the load torques are lower than the rated motor torque. As has already been demonstrated, decoupling control of motor speed and rotor flux is possible using multiscalar model-based nonlinear control. A straightforward method is described to choose the right flux level while considering copper loss and iron loss to increase steady-state motor efficiency, and are temperature-dependent and dependent on speed (w_{11}) and torque (w_{12}).

The iron loss is the sum of eddy-current loss and hysteresis;

$$P_{Rc} = P_{Rc}(eddy - current\ loss) + P_{Rc}(hysteresis\ loss) \tag{20}$$

$$P_{Rc}(eddy - current\ loss) = k_e(\omega^2 w_{21})$$

$$P_{Rc}(hysteresis\ loss) = k_h(\omega w_{21}) \tag{21}$$

where ω, stator angular frequency, k_e and k_h are the coefficients of the eddy-current loss and the hysteresis losses.

It is crucial that the eddy current loss outweighs the hysteresis loss in a high-frequency zone. Therefore, it is possible to approximate the stator iron loss $P_{Rc}(s)$ and the rotor iron loss $P_{Rc}(r)$ in the following manner [24]:

$$P_{Rc}(s) = (k_e\omega^2 + k_h\omega)w_{21} \approx (\frac{\omega^2 w_{21}}{1/k_e}) = \frac{\omega^2 w_{21}}{R_c} \tag{22}$$

$$P_{Rc}(r) = (k_e s^2\omega^2 + k_h s\omega)w_{21} \approx (\frac{s^2\omega^2 w_{21}}{1/k_e}) = \frac{s^2\omega^2 w_{21}}{R_c} \tag{23}$$

where s, motor slip, R_c is core loss equivalent resistance which is normally measured by no-load testand $1/k_e$ has the dimension of resistance.

Rotor iron loss can be neglected since $|s\omega| << |\omega|$ and now the total power loss can be written as;

$$P_L = \frac{3}{2}[R_s(i_{s\alpha}^2 + i_{s\beta}^2) + R_r(i_{r\alpha}^2 + i_{r\beta}^2)] + \frac{\omega^2 w_{21}}{R_c} \tag{24}$$

Solving for the rotor currents;

$$i_{r\alpha} = \frac{\phi_{m\alpha}}{L_r - L_m} - \frac{L_m i_{m\alpha}}{L_r - L_m}$$

$$i_{r\beta} = \frac{\phi_{m\beta}}{L_r - L_m} - \frac{L_m i_{m\beta}}{L_r - L_m} \tag{25}$$

Now writing the square of the stator and rotor currents in (24) in terms of multiscalar variables, the total power loss (P_L) can be written as:

$$P_L = \sigma_1\frac{w^2_{12}}{w_{21}} + \sigma_2 w_{21} \tag{26}$$

where;

$$\sigma_1 = (R_s L_r{}^2 + R_r L_m{}^2)/L_r{}^2$$

$$\sigma_2 = (R_s/L_m{}^2) + (\omega^2/R_c) \tag{27}$$

When the multiscalar variable w_{21} is at steady state, the loss minimization condition is given by;

$$\frac{\partial P_L}{\partial w_{21}} = 0 \tag{28}$$

The solution to the differential equation (26) is,

$$w_{21}\_optimum = \sqrt{\frac{\sigma_1}{\sigma_2}}\ |w_{12}| \tag{29}$$

where σ_1 and σ_2 are both calculated to be positive real numbers.

B. OBSERVER DESIGN

The proposal for the AFO design process was made in [16]. The following can be used to determine the AFO speed observer based on the IM mathematical model for ($\alpha\beta$) form.

$$\frac{d\hat{i}_{s\alpha}}{dt} = a_1\hat{i}_{s\alpha} + a_2\hat{\phi}_{m\alpha} + a_3\hat{i}_{m\alpha} + a_4 u_{s\alpha} + \Delta i_1 + z_\alpha$$

$$\frac{d\hat{i}_{s\beta}}{dt} = a_1\hat{i}_{s\beta} + a_2\hat{\phi}_{m\beta} + a_3\hat{i}_{m\beta} + a_4 u_{s\beta} + \Delta i_1 + z_\beta \tag{30}$$

$$\frac{d\hat{\phi}_{m\alpha}}{dt} = a_5\hat{\phi}_{m\alpha} + a_6\hat{i}_{m\alpha} - \hat{\omega}_r\hat{\phi}_{m\beta} + z_{\phi\alpha}$$

$$\frac{d\hat{\phi}_{m\beta}}{dt} = a_5\hat{\phi}_{m\beta} + a_6\hat{i}_{m\beta} - \hat{\omega}_r\hat{\phi}_{m\alpha} + z_{\phi\beta} \quad (31)$$

$$\frac{d\hat{i}_{m\alpha}}{dt} = a_7\hat{\phi}_{m\alpha} + a_8\hat{i}_{m\alpha} + a_9\hat{i}_{s\alpha} + \Delta i_1 + z_\alpha$$

$$\frac{d\hat{i}_{m\beta}}{dt} = a_7\hat{\phi}_{m\beta} + a_8\hat{i}_{m\beta} + a_9\hat{i}_{s\beta} + \Delta i_2 + z_\beta \quad (32)$$

where the estimated values are indicated by "^" and the stabilizing functions $z_{\alpha,\beta}$ and $z_{\phi\alpha,\beta}$ are added to the structure and $\Delta i_{1,2}$ are bounded parametric uncertain terms added exclusively to the stator and magnetizing current derivatives.

$$z_\alpha = -(\lambda_a + \Delta i_1)(e_{is\alpha/m\alpha})$$

$$z_\beta = -(\lambda_a + \Delta i_2)(e_{is\beta/m\beta}) \quad (33)$$

where $e_{is\alpha/m\alpha}$, $e_{is\beta/m\beta}$, are stator or magnetizing $\alpha - \beta$ component current errors between their actual and estimated values. The flux component stabilizing functions are;

$$z_{\phi\alpha} = -\gamma_1 e_{is\alpha} + \gamma_2\hat{\omega}_r e_{is\beta}$$

$$z_{\phi\alpha} = -\gamma_1 e_{is\beta} - \gamma_2\hat{\omega}_r e_{is\alpha} \quad (34)$$

where λ_a, γ_1, γ_2 are observer tuning gains (feedback gains) which are in (30)–(32) are chosen by pole placement method of linearized observer structure which is discussed in detail under stability analysis section.

The integrator can be used to replicate the value of rotor speed from an adaptive mechanism [16] as,

$$\frac{d\hat{\omega}_r}{d\tau} = \xi a_3(\hat{\phi}_{m\alpha}(i_{s\beta} - \hat{i}_{s\beta}) - \hat{\phi}_{m\beta}(i_{s\alpha} - \hat{i}_{s\alpha})) \quad (35)$$

where ξ is adaptation tuning gain.

C. STABILITY ANALYSIS

For the various IM operations, the stability property of speed estimation in the AFO structure was investigated, and the authors of [9] used the Routh-Hurwitz criterion to establish the necessary requirements for accurate speed estimation. The design approach for adaptation gain is displayed in [9]. The stability study of the IM model's ideal speed observer is conducted based on the studies mentioned in [9]. In this analysis (feedback gains), the linearized observer structure's pole placement method selects the observer tuning gains. These gains influence the rate of observer convergence. The observer structure can be linearized close to equilibrium points, or the tuning gains can be determined from the model of the observer errors, which is a nonlinear approach, or near equilibrium points, from the observer structure, which can be linearized.

The other stability analysis of the speed estimation in the AFO structure was presented in [16] by improving some of the limitations that occurred with [9], showing how various tuning gains affect the linearized observer system's stable operating range when there is additional feedback. In [16], to show how the value of various gains affects the placement

of observer poles, the tuning gains are chosen arbitrarily (extreme values of the tuning gains are used). However, none of them includes the effect of iron or core loss resistance in their mathematical model of the IM and the AFO observer structure, and the control system proposed in this article is different, having the inherent behavior of eliminating nonlinearity.

The coefficients $\lambda\alpha$ and ξ were introduced to stabilize the system. The general form of the linearized system is;

$$\frac{d}{dt}\Delta\mathbf{x}(t) = \mathbf{A}\Delta\mathbf{x}(t) + \mathbf{B}\Delta\mathbf{u}(t) \quad (36)$$

where $\mathbf{A}$ and $\mathbf{B}$ are the Jacobian matrices of state space representation and $\Delta\mathbf{x}(t)$, is estimation errors of stator currents, magnetizing fluxes, magnetizing currents and speed, and $\Delta\mathbf{u}(t)$ is treated as known control inputs.

The solution to (41) is given by;

$$\Delta\tilde{\mathbf{i}}_s = [s\mathbf{I} - \mathbf{A}]^{-1}\Delta\mathbf{A}\mathbf{x} \quad (37)$$

In some cases, the eigenvalues of the matrix are assessed at various operating points.

Case 1) $\omega_r = -1\ldots 1$, $\lambda_\alpha = 5$, $\gamma_1 = 0.4$, $\xi = 0.2$, $\gamma_2 = 0$ (where these parameters are included in matrix $\mathbf{A}$).

The spectrum of the matrix for the linearized observer system during the machine rotor speed change from -1.0 to 1.0 p.u. is displayed in fig. 3. Nominally, the machine is loaded at $T_L = 0.7$ p.u. If $\gamma_2 = 0$, fig.3. demonstrates that the AFO structure is unstable. Just a few of the observer poles have positive values while the system is in regenerating mode. For the feedback matrix gains equal to zero, however, for $\zeta = 0$, $\mu = 0$, this scenario was discussed in previous work. The feedback in the integrator structure is added to stabilize the AFO structure.
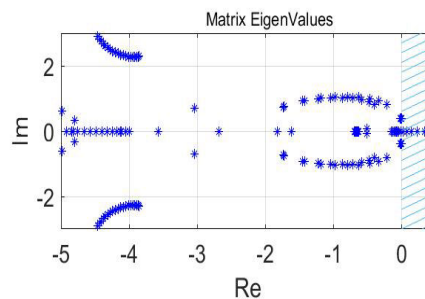

FIGURE 3. Spectrum of matrix of the linearized observer.

Case 2) $\omega_r = -1\ldots 1$, $\lambda_\alpha = 4$, $\gamma_1 = 0.2\ldots 4$, $\zeta = 0.2$, $\gamma_2 = 0.3\ldots 4$.

The additional term is proven to be included in order to move poles from unstable regions to stable ones. The state estimations, however, may oscillate if different tuning gain levels are selected. As demonstrated in the figures, the imaginary values of poles should be as close to zero as possible to reduce these oscillations. The coefficient γ_2 is a factor that affects where the poles of the linearized observer structure are located.

Fig.4. shows the effects of changing γ_2 from 0.5 to 4.0 for rotor speed from -1 to 1 p.u. and $T_L = 0.7$ p.u. on observer stability. The oscillation in the observer system (where imaginary value poles move away from zero) happens for increasing values of ζ.
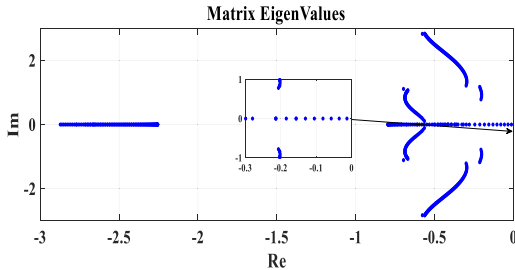

FIGURE 4. Spectrum of matrix of the linearized AFO observer system.

To show how the value of various gains affects the location of observer poles, the tuning gains are selected arbitrary (that is, their extreme values are picked).

IV. EXPERIMENTAL RESULTS

A voltage source converter (VSC)-powered 5.5 kW drive system was used for experiment. The electric drive system's parameters are listed in Table 1. The control system was created using a DSP Sharc ADSP21363 floating-point signal processor and an Altera Cyclone 2 FPGA. The transistor switched at a frequency of 3.3 kHz. 150 seconds were chosen as the sample duration. Using current transducers LA 25-NP, the stator current was measured in phases "a" and "b" before being transformed to the (α, β) reference frame using the Park transformation.

Using the induction motor with the following nominal parameters in table 1 and controller tuning gains in table 2, the verification of the proposed control is done experimentally.

TABLE 1. IM parameters and references unit.

Quantity	Symbol	Values
Stator resistance	Rs	2.92Ω
Rotor resistance	Rr	3.36Ω
Core resistance	Rc	682.56Ω
Magnetizing inductance	Lm	0.422H
Stator, rotor inductances	Ls,Lr	0.439H
Leakage inductance	Lls	0.017H
Nominal Power	Pn	5.5 kW
Nominal stator voltage	In	11 A
Nominal stator current	Un	400 V
Nominal rotor speed	n	1430 rpm
Nominal frequency	f	50 Hz
Reference current	$Ib= In\sqrt{3}$	19 A
Reference voltage	$Ub=Un$	400 V
Reference power	Pb	7.6 kW

Implementing the loss minimization model, the induction motor should be managed so that the necessary air gap is maintained at the necessary level, as far away from the stator frequency or stator current as is practicable. It is advised to

TABLE 2. Sensorless control system tuning gains.

Multiscalar variables and PI controller tuning gains					
Variables	$w_{11}(\omega_r)$		$w_{12}(T_e)$		$w_{21}(\phi^2_{m\alpha})$
Tuning gains	k_{p11}	k_{i11}	k_{p12}	k_{i12}	k_{p21}	K_{i21}
Values (p.u.)	6	0.01	10	0.01	5	0.028
Speed observer tuning gains					
Notations		λ_a	γ_1	ξ	γ_2
Values		0.001	1.1	0.9	1.08

maintain the airgap flux at its rated value for the quick drive reaction to reduce the time required for torque buildup.

Fig. 5. and 6. shows that the created torque has a decent starting speed and that, for the reference speed of 1 p.u, both the positive and negative portions of the predicted speed follow the actual speed. Compared to the controller without the core loss, the created torque has a smaller harmonic disturbance and settles to zero in a very short time.
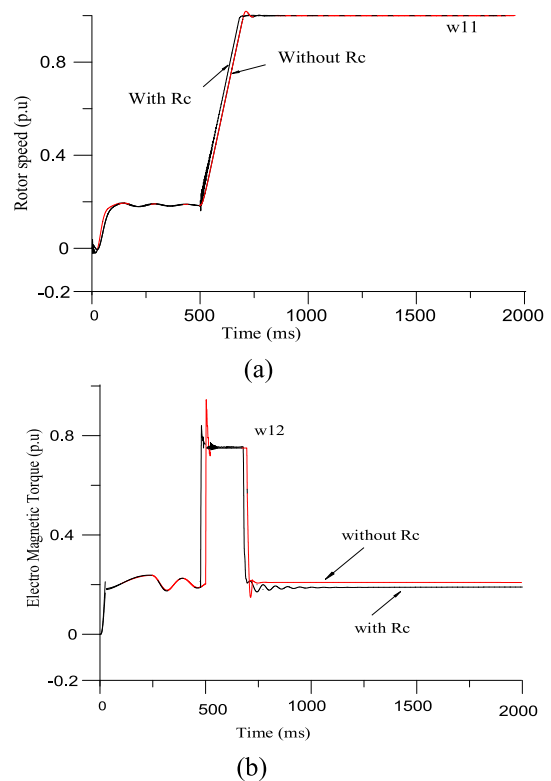

(a)

(b)

FIGURE 5. (a) Unloaded IM is starting up to $1(w_{11})$ and (b) electromagnetic torque (w_{12}).

As can be seen from fig. 8. below, the ideal flux levels provide lower values than when loss minimization is not considered. On the other hand, the flux demand is higher when loss-minimizing control (LMC) is not considered than when it is. The excess flux will necessitate needless increases in current, which implies an increase in the power wasted in the copper and core.
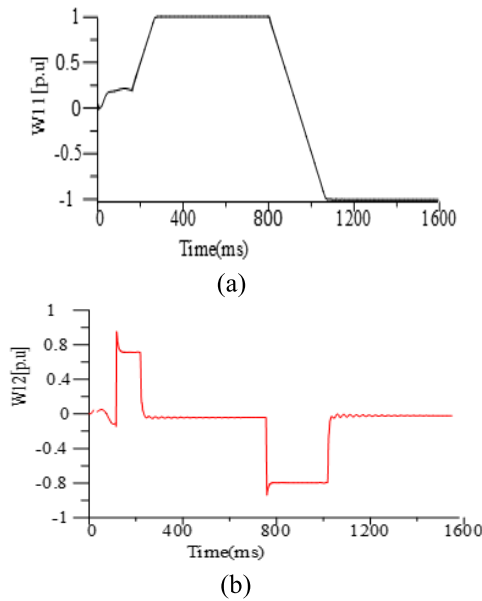
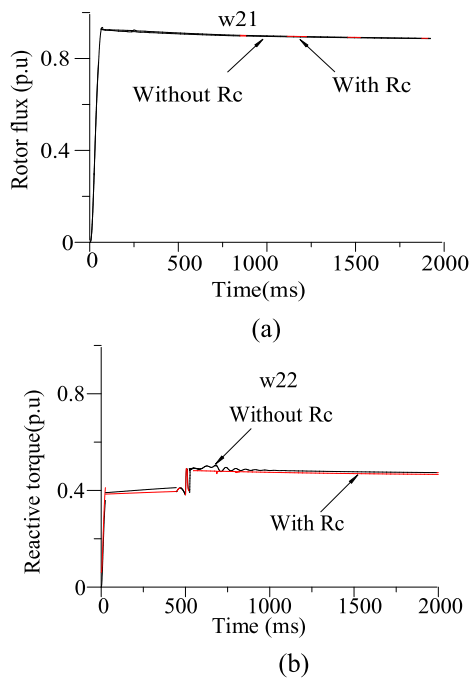FIGURE 6. (a) Unloaded IM is reversing to −1(w_{11}) and (b) electromagnetic torque (w_{12}).

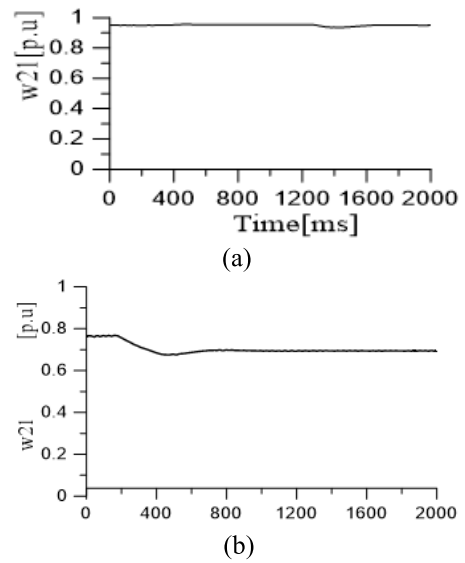FIGURE 7. (a) Square of rotor flux and (b) reactive torque.

FIGURE 8. Comparison of unoptimized (a) with optimized (b) flux.
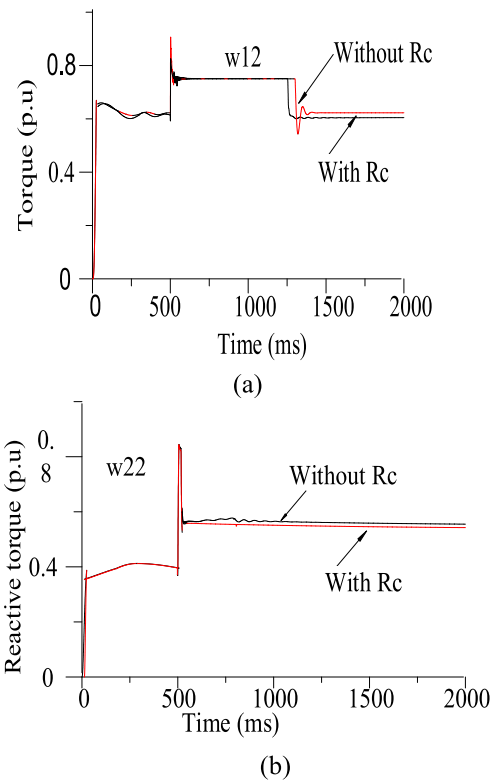
FIGURE 9. (a) Electromagnetic torque (w12) and (b) reactive torque component (w22).

A. RESULTS UNDER LOAD VARIATION

Fig.9. below shows the performance of the suggested system under various loads. When core loss resistance is considered, the system is more resistant to the load torque than when it is not, as demonstrated by applying $T_L = 0.4$ N-m load torque.

The performance of the suggested system is displayed for various loads applied to it in Fig. 10 below. The application of 0.6 N-m load torque shows that the system is more resistant to the load torque when core loss resistance is

taken into account than when the system is without core loss resistance.

Fig.14. shows the machine starting up to nominal speed with constant reference flux. At some point, the loss-minimizing flux model (LMC) is applied to reduce loss without affecting the machine running.

As it can be seen from fig. 15, the core loss is about 0.015 (p.u) which is about 82.5W without applying the LMC
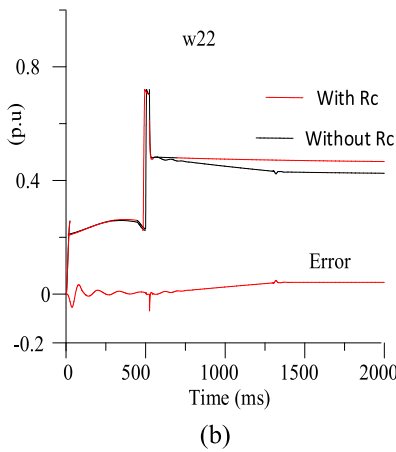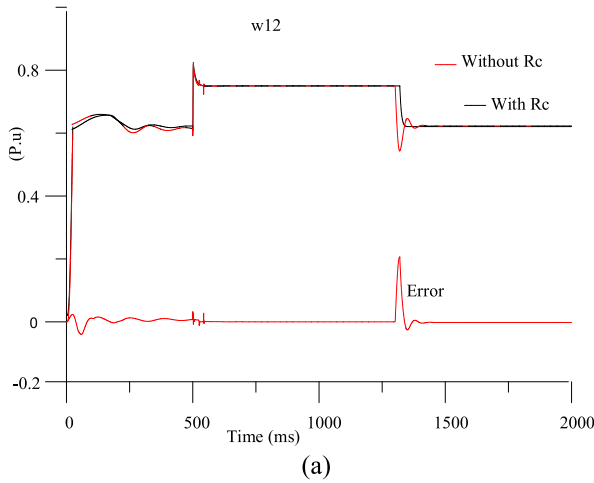
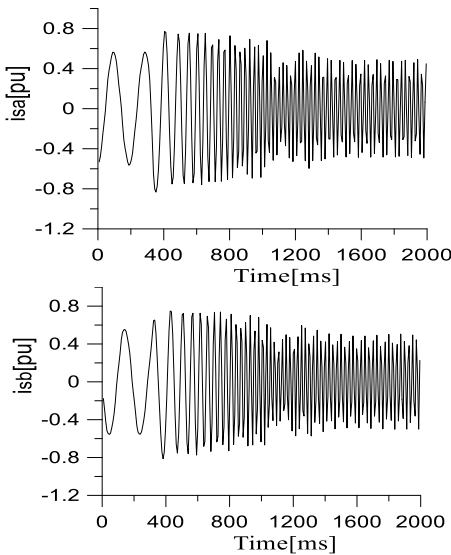FIGURE 10. (a) Electromagnetic torque (w12) and (b) reactive torque component (w22).

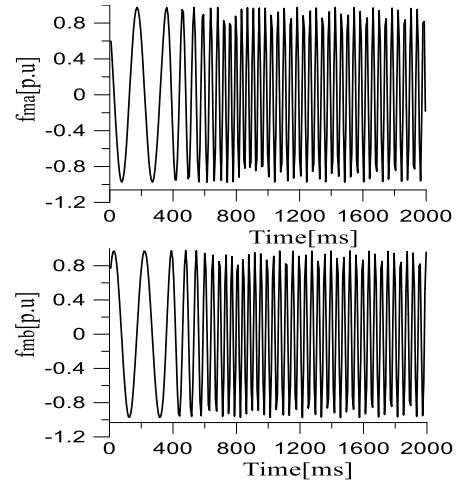
FIGURE 11. $\alpha, \beta -$stator currents.

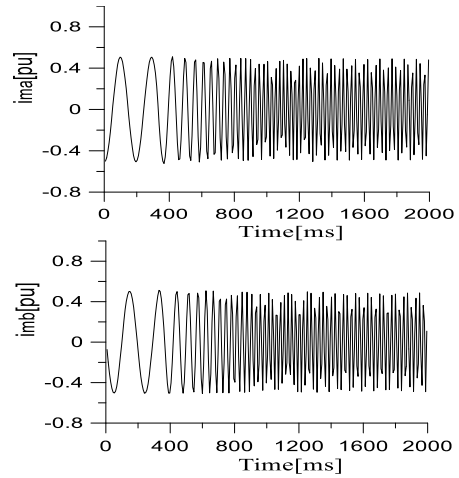FIGURE 12. $\alpha\beta$-airgap fluxes.

FIGURE 13. $\alpha\beta$-magnetizing currents.

TABLE 3. The error between the speed with R_c (w11$_{Rc}$) and without (w11), electromechanical torque with R_c (w12$_{Rc}$) and without (w12), flux square with R_c (W21$_{Rc}$) and without (w21), reactive torque with R_c (w22$_{Rc}$) and without (w22).

w11$_{Rc}$–w11 (e11)	w12$_{Rc}$–w12 (e12)	w21$_{Rc}$–w21 (e21)	w22$_{Rc}$–w22 (e22)
0	0	0	0.0015
0	0	0	0.0066
-0.0001	0	0	0.0325
0.0003	0	0	0.0325
0.0098	0.0002	0.0001	0.0825
0.0098	0.0007	0.0006	0.0825
0.0537	0.0007	0.0021	0.1161
0.0537	0.0012	0.0021	0.1544
0.0996	0.0017	0.0034	0.0015

and after applying LMC the core loss is reduced to 0.013 (p.u) which is 71.5w. This is significant amount in energy loss minimization and hence efficiency will increase.

From Fig. 16. below, it can be seen that stator copper loss is lower at a lower speed range and becomes higher when the speed rises, whereas the opposite happens with rotor
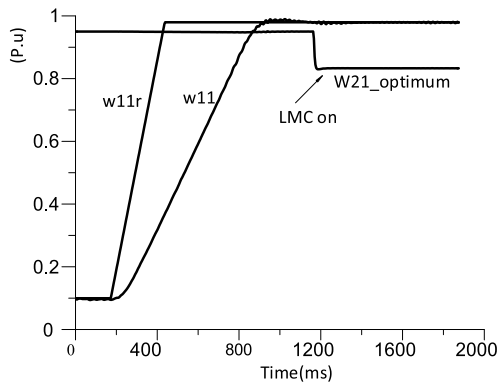
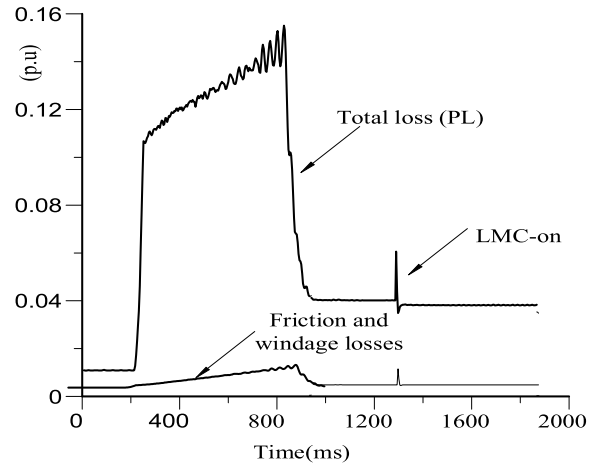**FIGURE 14.** Speed (w11), reference speed (w11r) and optimum flux (w21_optimum) when LMC is applied.

FIGURE 15. Speed (w11), and optimum flux (w21_optimum) when LMC is applied and core loss (PRc).

FIGURE 16. Stator and rotor copper losses.

FIGURE 17. Total and friction and windage losses.

FIGURE 18. Sensorless control system scheme.

FIGURE 19. Experimental stand with IM coupled to the dc-machine.

Figs. 18 and 19 are the overall sensorless control system and the laboratory setup views, respectively.

V. CONCLUSION

A loss-minimizing flux level control strategy for the IM drive was presented in this study. The loss minimization, flux estimation, and control of the IM involve magnetic saturation, hysteresis, and eddy-current losses. Based on this study, the optimal reference airgap flux power loss minimization algorithm has been constructed. Based on the developed model, a multiscalar control and a novel Lyapunov function for classical stability analysis have been used to design an observer-based controller that ensures asymptotic reference tracking for the velocity and optimal flux in the presence of load torque. Additionally, experimental implementation was completed to confirm the induction motor's excellent performance.
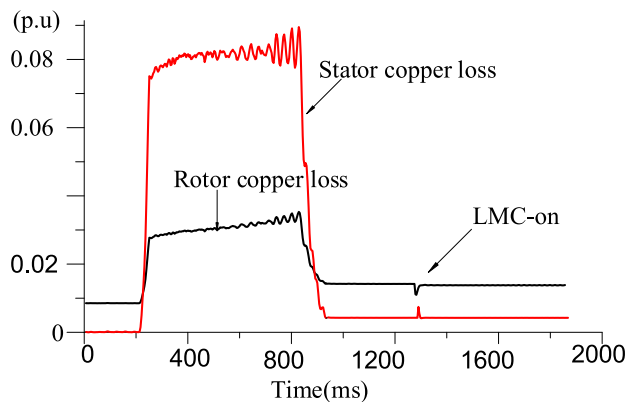
copper loss. Stator copper loss is about 0.03p.u (165W) and reduced to 0.012 p.u (66W) after applying LMC.

Fig. 17. below shows total loss (PL) 0.15 p.u (825W) and friction and windage losses of about 0.006p.u (33W) without applying LMC and 0.04p.u (220W) and 0.0012 p.u (6.6W) after LMC is applied respectively. It can be seen that when LMC is applied the whole components of the machine losses were reduced by significant amount and hence energy efficiency improvement or increment is attained.
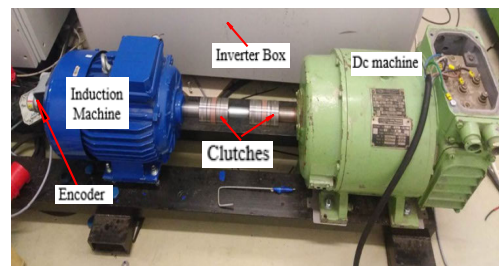
REFERENCES

[1] M. Morawiec, P. Kroplewski, and C. Odeh, "Nonadaptive rotor speed estimation of induction machine in an adaptive full-order observer," *IEEE Trans. Ind. Electron.*, vol. 69, no. 3, pp. 2333–2344, Mar. 2022, doi: 10.1109/TIE.2021.3066919.

[2] S. Di Gennaro, J. R. Domínguez, and M. A. Meza, "Sensorless high order sliding mode control of induction motors with core loss," *IEEE Trans. Ind. Electron.*, vol. 61, no. 6, pp. 2678–2689, Jun. 2014, doi: 10.1109/TIE.2013.2276311.

[3] T. Ayana, L. Wogi, and M. Morawiec, "Core loss resistance impact on sensorless speed control of an induction motor using hybrid adaptive sliding mode observer," *Arch. Electr. Eng.*, vol. 72, no. 4, pp. 895–913, 2023, doi: 10.24425/aee.2023.147417.

[4] J. Maneiro, R. Ryndzionek, T. Lagier, P. Dworakowski, and C. Buttay, "Design of a SiC based triple active bridge ceil for a multi-megawatt DC–DC converter," in *Proc. ECCE Europe*, Warsaw, Poland, Sep. 2017, pp. 1–10, doi: 10.23919/EPE17ECCEEurope.2017.8099005.

[5] P. Strankowski, J. Guzinski, M. Morawiec, A. Lewicki, and F. Wilczynski, "Sensorless five-phase induction motor drive with third harmonic injection and inverter output filter," *Bull. Polish Acad. Sci. Tech. Sci.*, vol. 68, no. 3, pp. 437–445, May 2020, doi: 10.24425/bpasts.2020.133369.

[6] Z. Krzeminski, "Nonlinear control of induction machines," in *Proc. 10th IFSC World Congr.*, Munich, Germany, 1987, pp. 349–354.

[7] Z. Yin, G. Li, Y. Zhang, and J. Liu, "Symmetric-strong-tracking-extended-Kalman-filter-based sensorless control of induction motor drives for modeling error reduction," *IEEE Trans. Ind. Informat.*, vol. 15, no. 2, pp. 650–662, Feb. 2019, doi: 10.1109/TII.2018.2810850.

[8] D. Lindenmeyer, H. W. Dommel, A. Moshref, and P. Kundur, "An induction motor parameter estimation method," *Int. J. Electr. Power Energy Syst.*, vol. 23, no. 4, pp. 251–262, May 2001, doi: 10.1016/S0142-0615(00)00060-0.

[9] S. Suwankawin and S. Sangwongwanich, "Design strategy of an adaptive full-order observer for speed-sensorless induction-motor drives-tracking performance and stabilization," *IEEE Trans. Ind. Electron.*, vol. 53, no. 1, pp. 96–119, Feb. 2006, doi: 10.1109/TIE.2005.862308.

[10] W. Sun, K. Liu, D. Jiang, and R. Qu, "Zero synchronous speed stable operation strategy for speed sensorless induction motor drive with virtual voltage injection," in *Proc. IEEE Energy Convers. Congr. Expo. (ECCE)*, Portland, OR, USA, Dec. 2018, pp. 337–343, doi: 10.1109/ECCE.2018.8557756.

[11] M. Hinkkanen and J. Luomi, "Stabilization of regenerating-mode operation in sensorless induction motor drives by full-order flux observer design," *IEEE Trans. Ind. Electron.*, vol. 51, no. 6, pp. 1318–1328, Dec. 2004, doi: 10.1109/TIE.2004.837902.

[12] M. Bouheraoua, J. Wang, and K. Atallah, "Rotor position estimation of a pseudo direct drive PM machine using extended Kalman filter," in *Proc. Conf. IEEE Energy Convers. Congr. Expo.*, Montreal, QC, Canada, Oct. 2015, pp. 292–299, doi: 10.1109/ECCE.2015.7309701.

[13] H. Kubota, K. Matsuse, and T. Nakano, "DSP-based speed adaptive flux observer of induction motor," *IEEE Trans. Ind. Appl.*, vol. 29, no. 2, pp. 344–348, Mar./Apr. 1993, doi: 10.1109/28.216542.

[14] H. Kubota and K. Matsuse, "Speed sensorless field-oriented control of induction motor with rotor resistance adaptation," *IEEE Trans. Ind. Appl.*, vol. 30, no. 5, pp. 1219–1224, Oct. 1994, doi: 10.1109/28.315232.

[15] E. Levi and M. Wang, "A speed estimator for high performance sensorless control of induction motors in the field weakening region," *IEEE Trans. Power Electron.*, vol. 17, no. 3, pp. 365–378, May 2002, doi: 10.1109/TPEL.2002.1004244.

[16] M. Morawiec and P. Kroplewski, "Nonadaptive estimation of the rotor speed in an adaptive full order observer of induction machine," *Bull. Polish Acad. Sci. Tech. Sci.*, pp. 973–981, Sep. 2020, doi: 10.24425/bpasts.2020.134654.

[17] F.-Z. Peng and T. Fukao, "Robust speed identification for speed-sensorless vector control of induction motors," *IEEE Trans. Ind. Appl.*, vol. 30, no. 5, pp. 1234–1240, Oct. 1994, doi: 10.1109/28.315234.

[18] K. L. Shi, T. F. Chan, Y. K. Wong, and S. L. Ho, "Speed estimation of an induction motor drive using an optimized extended Kalman filter," *IEEE Trans. Ind. Electron.*, vol. 49, no. 1, pp. 124–133, Feb. 2002, doi: 10.1109/41.982256.

[19] J. Rivera Dominguez, C. Mora-Soto, S. Ortega, J. J. Raygoza, and A. De La Mora, "Super-twisting control of induction motors with core loss," in *Proc. 11th Int. Workshop Variable Struct. Syst. (VSS)*, Jun. 2010, pp. 428–433, doi: 10.1109/VSS.2010.5544737.

[20] M. Mansouri, M. Mohamed-Seghir, H. Nounou, M. Nounou, and H. Abu-Rub, "Estimation of nonlinear control parameters in induction machine using particle filtering," in *Proc. 10th Int. Multi-Conf. Syst., Signals Devices (SSD13)*, Hammamet, Tunisia, Mar. 2013, pp. 1–7, doi: 10.1109/SSD.2013.6564095.

[21] Y. Kim, S. Sul, and M. Park, "Speed sensorless vector control of induction motor using extended Kalman filter," *IEEE Trans. Ind. Appl.*, vol. 30, no. 5, pp. 1225–1233, Oct. 1994, doi: 10.1109/28.315233.

[22] D. S. Kirschen, D. W. Novotny, and T. A. Lipo, "On-line efficiency optimization of a variable frequency induction motor drive," *IEEE Trans. Ind. Appl.*, vol. IA-21, no. 3, pp. 610–616, May 1985, doi: 10.1109/TIA.1985.349717.

[23] C. Chakraborty and Y. Hori, "Fast efficiency optimization techniques for the indirect vector-controlled induction motor drives," *IEEE Trans. Ind. Appl.*, vol. 39, no. 4, pp. 1070–1076, Jul. 2003, doi: 10.1109/TIA.2003.814550.

[24] M. Adamowicz and J. Guzinski, "Minimum-time minimum-loss speed sensorless control of induction motors under nonlinear control," in *Proc. IEEE Compat. Power Electron.*, Gdynia, Poland, Jun. 2005, pp. 1–7, doi: 10.1109/CPE.2005.1547546.

TADELE AYANA received the B.Sc. degree in electrical and computer engineering from Jimma University, in 2013, and the M.Sc. degree in control and instrumentation engineering from the Jimma Institute of Technology, Jimma, Ethiopia, in 2018. He is currently pursuing the Ph.D. degree with the Faculty of Electrical and control Engineering, Department of Electric Drives and Energy Conversion, Gdańsk University of Technology, Gdańsk, Poland. Since 2018, he has been a Lecturer with the Jimma Institute of Technology. He is the author of more than five articles. His main research interests include multiscalar models, nonlinear control of electrical machines, sensorless control, nonlinear control, adaptive observer, and sliding mode control.

MARCIN MORAWIEC (Senior Member, IEEE) received the M.Sc. degree in electrical engineering from the Częstochowa University of Technology, Poland, in 2003, the Ph.D. degree from the Gdańsk University of Technology, Gdańsk, Poland, in 2007, and the D.Sc. degree in electrical drives, in 2017. He is currently a Professor with the Gdańsk University of Technology. He is the author of more than 70 articles and two monographs and two chapters in books, one Polish patent, and five patent applications. His main research interests include multiscalar models, nonlinear control of any electrical machines, sensorless control, nonlinear control, backstepping control, adaptive observer backstepping, and sliding mode control.

LELISA WOGI received the B.Sc. degree in electrical and computer engineering from Jimma University, in 2017, and the M.Sc. degree in control and instrumentation engineering from the Jimma Institute of Technology, Jimma, Ethiopia, in 2022. Since 2017, he has been an Assistant Lecturer with Bule Hora University. He is currently pursuing the Ph.D. degree with the Faculty of Electrical and Control Engineering, Department of Electric Drives and Energy Conversion, Gdańsk University of Technology, Gdańsk, Poland. He is the author of more than three articles. His main research interests include nonlinear control of electrical machines, sensorless control, nonlinear control, adaptive observer, and sliding mode control.

● ● ●